Fig. 26.24
PBT gain as a function of applied voltage. The amplitude was measured using the electro-optic sampling system.

REFERENCES

1. J. A. Valdmanis, G. Mourou, and C. W. Gabel, *Appl. Phys. Lett.* **41**, 211 (1982).

2. K. E. Meyer, D. R. Dykaar, and G. A. Mourou, in *Picosecond Electronics and Optoelectronics*, edited by G. A. Mourou, D. M. Bloom, and C. H. Lee (Springer-Verlag, Berlin, Heidelberg, New York, and Tokyo, 1985), p. 54.

3. C. O. Bozler *et al.*, in *Proc. 7th Bien. Cornell Conf. on Active Microwave Devices*, p. 33 (1979).

4. M. A. Hollis *et al.*, *Technical Digest IEDM*, p. 102 (1985).

3.B Nodular Defects in Optical Coatings

Damage in transport optics for high-peak-power lasers often occurs first at defect sites in optical coatings. A characteristic defect in coatings is the nodule. It causes scattering and moisture penetration; in high-energy laser coatings, the localized stress,[1] localized heat,[2] and microlens effects[3] generated by nodules are assumed to trigger laser-induced damage. Nodular defects are found in various metal and dielectric films that are fabricated by sputtering, chemical vapor deposition, electroplating, thermal evaporation (both electron beam and thermal resistive), and ion plating.

A number of reports have focused on this microstructure during the last 15 years. K. Guenther[4] outlined the importance of the nodule in

optical coatings. Nodular defects[5] were thought to be formed by the same self-shadowing effects that cause columnar structure.[4,5] However, this effect alone could neither explain the nodular growth in films deposited at normal incidence nor the peculiar shapes of nodules. This report investigates the character, formation, and development of nodular defects in thin films. Computer simulation and experimental verification of nodule growth are emphasized.

By using a modified version of the hard-disk model, this simulation maintains the simplicity that is essential in simulating film growth on a large scale (up to 120,000 deposited disks). The modified model can accommodate different deposition conditions and material properties and thereby link the growth of nodules to these conditions.

The starting point of these calculations is the two-dimensional hard-disk model of Dirks and Leamy,[6] in which disks fall randomly onto the surface and then stick where they land or come to rest in the nearest pockets, where each disk is supported by two other disks that had arrived earlier. Results from this model reproduce well the experimentally found appearance of columnar microstructure and columnar tilt in thin films. The model best reproduces low-density films and inherently favors hexagonal, close-packed structures. However, it fails to take account of complex adsorption processes that influence film-structure evolution. During actual condensation, an adatom or admolecule moves some distance over the surface after impact because of transverse momentum conservation and thermal diffusion.[7] This migration of adatoms and admolecules depends critically on substructure temperature, kinetic energy of incident particles, residual-gas content, surface topography, and adatom and admolecule activation energies.

The modified model (Fig. 26.25)[8,9] includes the migration process by allowing an incident disk to migrate across the surface by jumping from site to site until an eligible site is reached. A probability-density distribution is established for the likelihood of a newly arriving disk undertaking 1, 2, or n jumps after impact and before coming to rest. R_1, R_2 . . . R_n are the probabilities for 1, 2 . . . n sequential jumps, satisfying

$$\sum_{j=1}^{n} R_j = 1 . \tag{1}$$

The migration parameter λ combines this probability density with the average distances covered by the jumping disks for 1, 2 . . . or n jumps:

$$\lambda = 0.6\,R_1 + 1.6\,R_2 + \quad . \quad . \quad . \quad + a_n R_n \quad , \tag{2}$$

where the coefficients a_n are the average distances traveled by the disks. These distances are derived from a separate set of simulations. In simulating different adatom-mobility conditions, a suitable value for the migration parameter λ is chosen, and restrictions are imposed on the probability distribution in order to come up with a set of values for the R_n.

Molecular dynamics models of surface effects, such as film growth or roughening, often use a Lennard-Jones interaction potential in describing the forces among the lattice constituents. Here a simplified representation of this potential is chosen for reasons of computational speed. It constitutes a compromise between the simplest hard-disk interaction — i.e., one in which the attractive force is constant up to twice a disk radius and in which the disks have to touch before the force acts — and the computationally unwieldy, full Lennard-Jones interaction. This code uses a constant force that is truncated in range by an adjustable extension factor that is heuristically set between 1 and 1.75. Disks passing within this extended capture length are attracted to the fixed disks.

The film-growth simulation code has been implemented on IBM-XT and HP 9000-200 microcomputers. By adjusting various parameters one can create a coating with nodules in "controlled conditions." Experiments in support of the simulation activities used Al_2O_3 grains, whose diameters were larger than 0.05 μm, as seeds for nodule growth on polished glass surfaces. The seeded substrates were overcoated with either a single layer of ZnS or multilayer Ta_2O_5–SiO_2 stacks. Both normal incidence on stationary substrates and various oblique-incidence angles for rotating substrates were explored. The samples were fractured, and coating cross sections were examined by SEM.
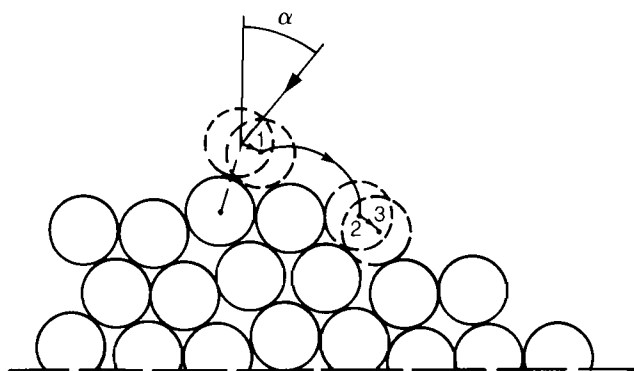
α = vapor incidence angle
λ = average distance jumped by hard disks

G1625
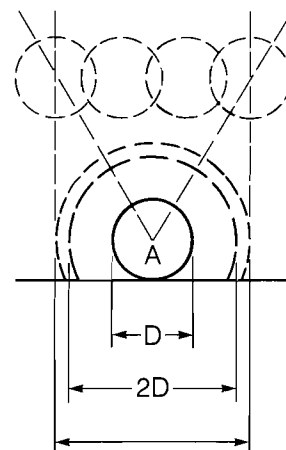
2D × extending factor

G1755

Fig. 26.25
Modified hard-disk model allows multiple jumps of an adatom after it impinges on the substrate. In this example, the adatom was allowed to jump three times before coming to rest.

Fig. 26.26
An approximate potential is implemented by extending the capture length of an adatom. In the hard-disk model, the capture length is just two times the radius of the adatom. In our model, we extend this length by a factor ranging from 1 to 1.75.

The Self-Extending Effects of Clusters and Nodules

Almost all nodule shapes found in thin films are characterized by an inverted cone with a dome or egg-like top. Their diameter increases monotonically with film thickness. Such nodule-like growth occurs even when the effects of the surrounding film are ignored. In this case we refer to the isolated growth structures as clusters. Nodules and clusters show self-extension, which can be examined by varying the capture length during the growth process.

A disk, A, has a capture length greater than its diameter, as shown in Fig. 26.26. Newly arriving disks within this capture length will impinge upon A such that the cluster starting at disk A extends its diameter during growth and forms a cone regardless of specific seed size or adatom mobility. The cone angle of clusters that form on an individual disk is $36° \pm 2°$ at $\lambda = 0$, as shown in Fig. 26.27(a), and is almost the same result as P. Ramanlal's disk fan.[10] The cone angles vary from $30°-40°$ if clusters initiate at larger-circle seeds [Fig. 26.27(b)].

The effects of extending the capture length, when adatom mobility is accounted for, are seen in Figs. 26.27(c) and 26.27(d). The increase in mobility results in a decrease of the cone angle of the cluster when the capture length is not extended. However, if the capture length of the disks is extended, the nodule cone angle of the cluster increases. This suggests that longer-range attractive forces between atoms produce larger cone angles.

Clusters forming simultaneously and in close proximity to one another on a smooth substrate will not initiate the self-extending process in the computer simulations because of competition among adjacent clusters. Nodules do not form spontaneously from homogeneous nucleations on a smooth substrate surface for the same reason. Only those clusters that start at protrusive seeds have chances to develop the nodule shapes.

The Geometry of Nodule Growth

A growth simulation of a nodule on a stationary substrate is shown in Fig. 26.28(a). The structure is characterized by straight sides similar to those of Fig. 26.28(b) (single layer of ZnS) and Fig. 26.28(c) (multilayer of Ta_2O_5-SiO_2). The nodule cone angle in Fig. 26.28(c) is $42°$, close to the one with an extending factor 1.5 in Fig. 26.27(d). The thickness of the simulated film in Fig. 26.28(a) is about 1700 Å if a disk represents an atom of diameter 5 Å.

Figure 26.29(a) is a simplified case of the initial stage of cluster growth on a rotating substrate with oblique vapor incidence ($\alpha = 50°$). Any point on the nodule side is exposed to the incident flux during half of a rotation period so that the seed grows with a cone angle 2γ. J is the incident flux and the cone angle γ satisfies

$$\tan\gamma = \frac{\int_{-\pi/2}^{\pi/2} J \sin(\alpha - \gamma)\, d\phi}{\int_{0}^{2\pi} J \cos\alpha\, d\phi} \qquad (3)$$

(a)   nucleus: single disk
        $\lambda = 0, \ \theta = 36° \pm 2°$

G1626

(b)   nucleus: circle
        $\lambda = 0, \ \theta = 30° \sim 40°$

(c) $\lambda = 1.9, \theta = 20°$
        extending factor $= 1.0$

G1627

(d) $\lambda = 2.0, \theta = 45°$
        extending factor $= 1.5$
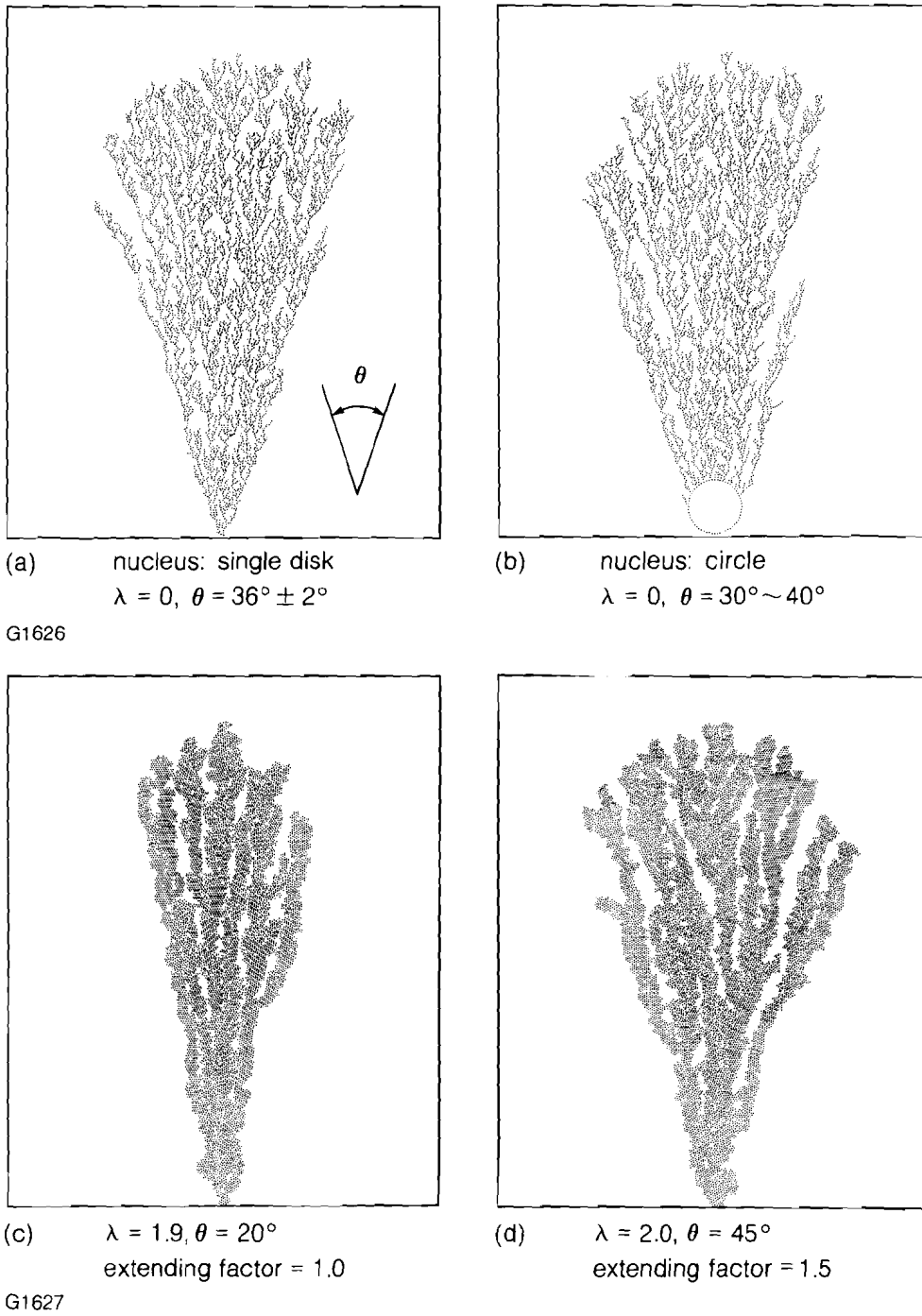
Fig. 26.27
Development of the model for simulating cluster growths in "free space." Growths with low adatom mobility are seen in (a) and (b), where the nucleus is a single adatom and a larger circle. Repeated trials of (a) gave consistent values for the cone angle. Allowing some adatom mobility results in a lower cone angle (c). Extension of the capture length (d) increases the cone angle.

No rotation
λ = 2.7, extending factor = 1.5

(a)

360 disks

G1629

(b)

|←————— 5 μm —————→|

G1631

(c)

|←———— 2 μm ————→|

G1630
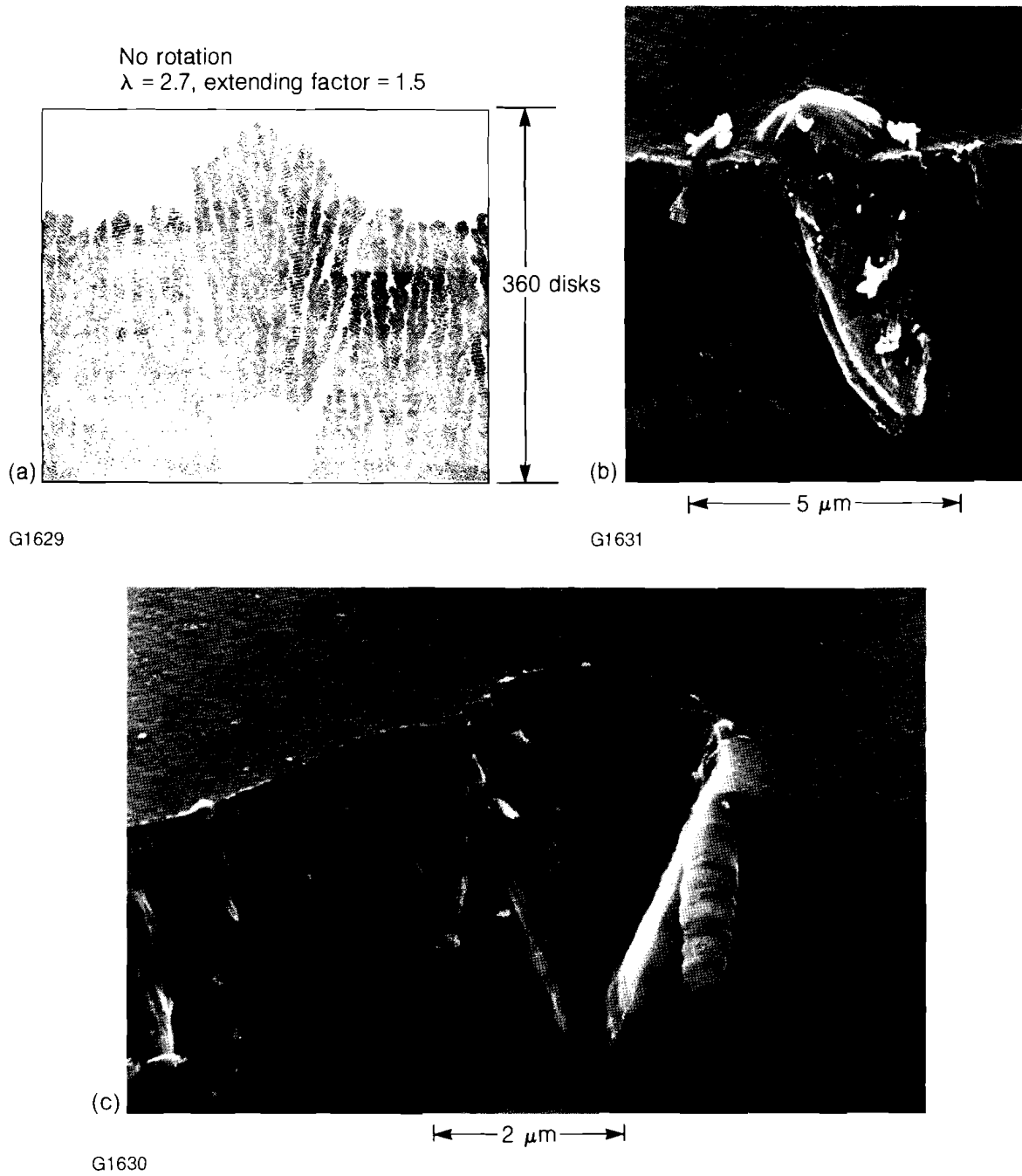
Fig. 26.28
The characteristic shape of a nodule formed on a fixed substrate with normal vapor incidence is an inverted cone. The model (a) is supported by experiment with single (b) and multiple (c) layer films.

$$\tan \gamma \simeq \frac{1}{(1 + \pi)} \tan \alpha$$

(a)

G1638

$\alpha = 50°, \lambda = 3.5$
extending factor = 1.5

(b)
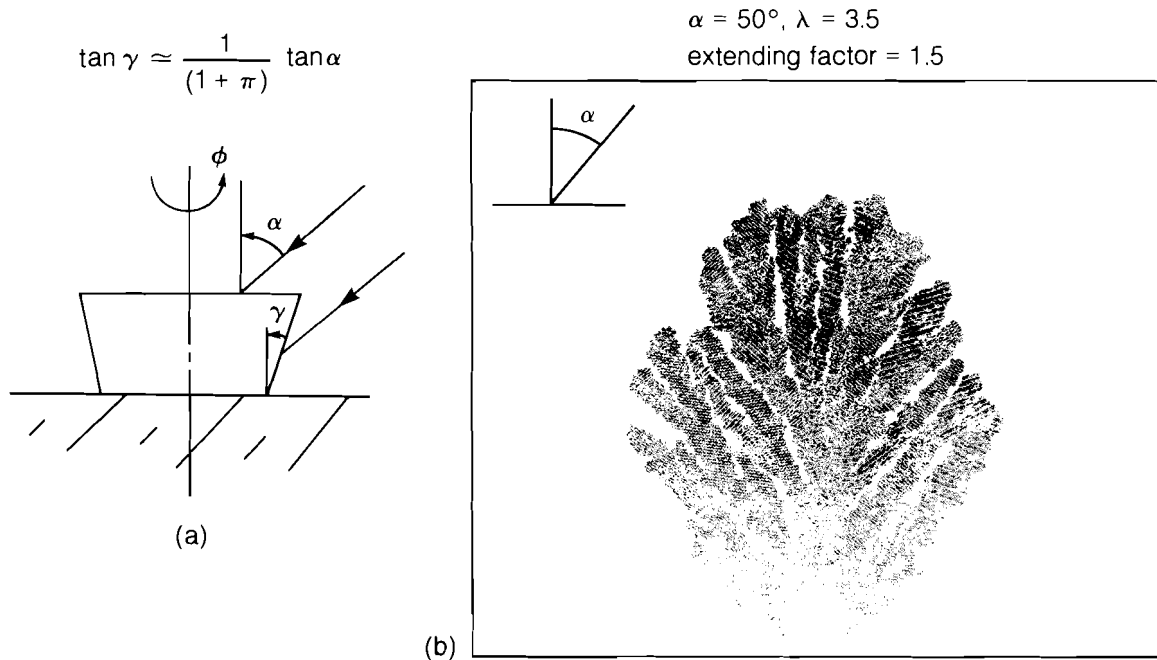
Fig. 26.29
Rotation of the substrate and an oblique vapor incidence results in an increase in the nodule cone angle. The simulation in (b) shows this effect for a nodule without the restrictive influence of the surrounding film. This is typical for the initial stages of nodule growth.

For small γ, the approximation holds

$$\tan \gamma \simeq \frac{1}{(1 + \pi)} \tan \alpha . \qquad (4)$$

Equation (3) establishes the relation between α and γ in a cluster forming on a rotating substrate. An increase in the incident angle α results in a corresponding increase in the cone angle γ. A cluster enlarges its diameter rapidly [Fig. 26.29(b)] during the early growth stage. In fact, Eq. (3) holds only at the initial stage of coating growth. After the step around a seed disappears and the dome on top of the nodule forms, the increase in nodule diameter slows down. As a result, a bowl-like bottom or parabolic sides evolve, in contrast to the straight sides of the nodules grown under normal incident flux on stationary substrates. Nodules in a coating deposited by a wide source (i.e., sputtering) exhibit similar shapes due to the spread in angle of incident particles typical for such a condition. Figures 26.30(a) and 26.31(a) are two nodule simulations for rotating substrates (on axis). Note that the diameter of the nodule grown at an angle of incidence $\alpha = 70°$ is much larger than that at $\alpha = 50°$. In Figs. 26.30(b) and 26.30(c) as well as Figs. 26.31(b) and 26.31(c), experimental test specimens are shown for comparison. Although the scale lengths are orders of magnitude different between simulations [Figs. 26.30(a) and 26.31(a)] and the corresponding micrographs [(b) and (c) of both figures], the visual agreement in geometry is quite good.
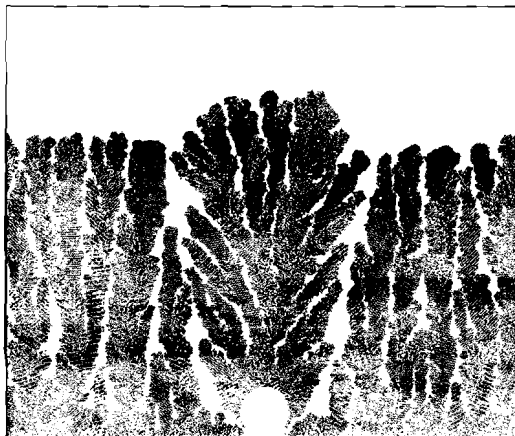
$\alpha = 50°$, $\lambda = 3.5$, extending factor = 1.5

Fig. 26.30
Nodule simulations and experiments on
rotating substrates at 45° vapor incidence.

(a)

G1635   Simulation

45° vapor incidence/single ZnS film

(b)

├────── 5 μm ──────┤

G1636

(c)
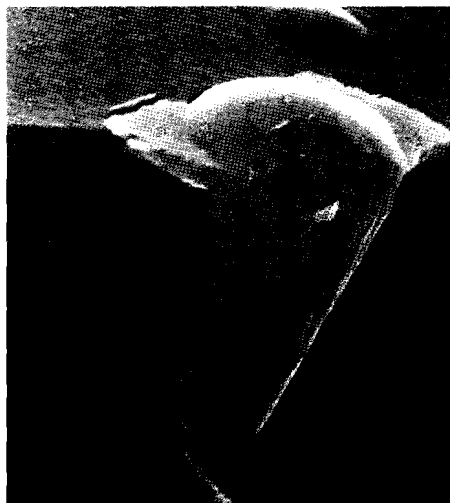
├────── 5 μm ──────┤

A seed is a necessary condition for a nodule to form. However, while larger seeds tend to generate larger nodules in simulations, not all seeds will grow into nodules. We find, for instance, that a seed of three-disk diameter fades into the film without nodule formation during growth at normal incidence. At sufficient adatom mobility (λ = 3.4), disks migrate longer distances along the surface and fill the volume around the small seed. Larger imperfections, such as dust, polishing residue, and rough protrusions on substrate surfaces, all act as starting points for nodules. Smaller defects on substrates, such as impurities, scratches,

95

$\alpha = 70°$, $\lambda = 3.5$, extending factor = 1.5
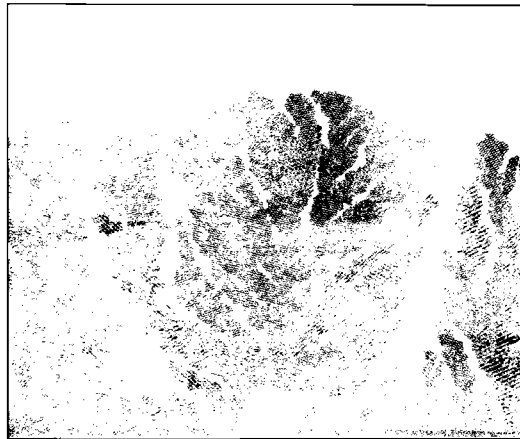
(a) Simulation

G1639

Fig. 26.31
*Nodule simulations and experiments at 70°
vapor incidence. The size of the nodules
varied significantly at this vapor angle.*

70° vapor incidence/single ZnS film

Small Seed

Large Seed

(b)

|◄——— 2 μm ———►|

(c)

|◄——— 5 μm ———►|

G1641
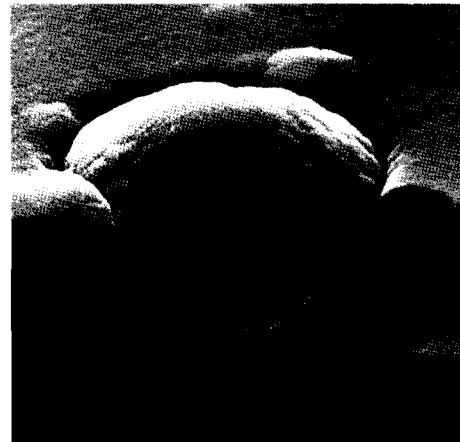
steps, and ledges, are preferred nucleation sites and may develop into seeds for nodules under suitable condensation conditions.

Figure 26.32 shows the simulation for a three-layer film containing a nodule that initiated at a spatter site in the first layer. It also shows the nodule growth through the layer interfaces.

The shadowing effect of a nodule produces an empty area around it during growth that causes a gap if addisks are not activated into filling

the volume. These gaps, which amount to 50 Å to 100 Å in corresponding simulations, depending on mobility, can be clearly seen around large nodules in the SEM micrographs of the film cross sections [Figs. 26.31(b) and 26.31(c)]. These gaps represent a significant break in a film's continuity. They also impede thermal conductance away from the nodule if, under high-power laser irradiation, the nodule's absorption should cause local heating.

$\alpha = 50°$, $\lambda = 3.7$, extending factor = 1.25, rotation
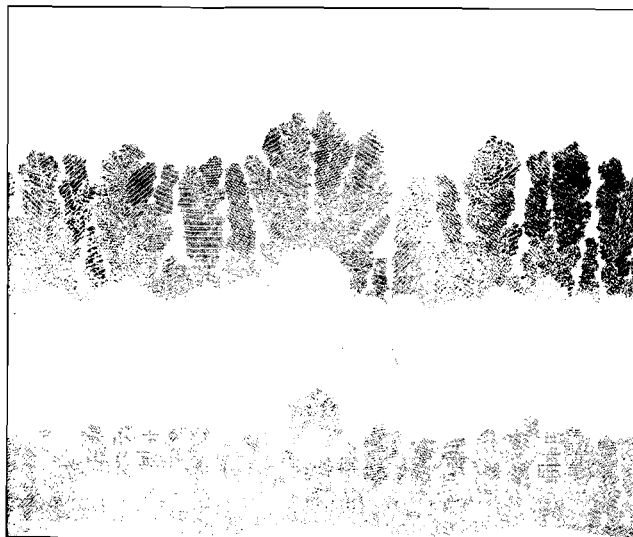
G1642

Fig. 26.32
Particles thrown up from the evaporant can act as nuclei for nodules. The nodule seen here also propagates up through a multilayer.

ACKNOWLEDGMENT

REFERENCES

1. T. Spalvins and W. A. Brainard, *J. Vac. Sci. Technol.* **11**, 1186 (1974).

2. K. H. Guenther, *Appl. Opt.* **23**, 3806 (1984).

3. J. Murphy, *Contemporary Infra-Red Sensors and Instruments* (SPIE, Bellingham, WA, 1980), Vol. 246, p. 64.

4. K. H. Guenther, *Appl. Opt.* **20**, 1034 (1981).

5. J. W. Patten, *Thin Solid Films* **63**, 121 (1979).

6. A. G. Dirks and H. J. Leamy, *Thin Solid Films* **47**, 219 (1977).

7. K. L. Chopra, *Thin Film Phenomena* (McGraw-Hill, New York, 1969), Chap. 4.

8. Liao Bangjun and H. A. Macleod, *Proceedings of the Southwest Conference on Optics* (SPIE, Bellingham, WA, 1985), Vol. 540, #TA 118.

9. Liao Bangjun and H. A. Macleod (to be published).

10. P. Ramanlal and L. M. Sander, *Phys. Rev. Lett.* **54**, 1828 (1985).